MDPI

*Article*

# Petrographic-Mineralogical Characterization of Archaeological Materials from "Casa di Diana" *Mithraeum* Sited in the Open Museum of Ostia Antica

Claudia Scatigno [1],*, Maria Preite Martinez [2], Nagore Prieto-Taboada [3], Juan Manual Madariaga [4,5] and Aida Maria Conte [6],*

1    CREF–Museo Storico della Fisica e Centro Studi e Ricerche "Enrico Fermi", Via Panisperna 89 a, c/o Piazza del Viminale 1, 00189 Rome, Italy
2    Department of Earth Sciences, Sapienza University of Rome, P.le Aldo Moro 5, 00185 Rome, Italy; mpreitem.mpm@gmail.com
3    Department of Applied Chemistry, Faculty of Chemistry, University of the Basque Country (UPV/EHU), Pº Manuel Lardizabal, 3, Basque Country, 20018 Donostia, Spain; nagore.prieto@ehu.eus
4    Department of Analytical Chemistry, Faculty of Science and Technology, University of the Basque Country (UPV/EHU), P.O. Box 644, Basque Country, 48080 Bilbao, Spain; juanmanuel.madariaga@ehu.eus
5    Unesco Chair of Cultural Landscapes and Heritage, University of the Basque Country UPV/EHU, P.O. Box 450, Basque Country, 01006 Vitoria-Gasteiz, Spain
6    CNR-IGAG, Department of Earth Sciences, Sapienza University of Rome, P.le Aldo Moro 5, 00185 Rome, Italy
*    Correspondence: claudia.scatigno@cref.it (C.S.); aidamaria.conte@uniroma1.it (A.M.C.)

**Abstract:** *Mithraea*, religious Roman buildings, are very common in Italian archeological sites. There are sixteen in *Ostia Antica* (Rome, Italy)The poor state of conservation, due to the intrinsic environmental conditions, characterized them: they consist of open-air museums and caves simultaneously. These places of worship are characterized by the presence of heterogeneous materials, such as wall building materials (bricks and mortars) and others used for furnishings and fittings. This increases the risk of accelerated damage because the materials 'rheology is different. Here, a full petrographic-mineralogical characterization with polarized light microscopy (PLM), X-ray diffraction (XRD), scanning electron microscope with energy dispersive X-ray (SEM-EDS) and isotopic analysis (δ13C, δ18O) is carried out on materials like travertine, marble, pumice, ceramic, and wall-building materials in "Casa di Diana" *Mithraeum* (Ostia Antica). Their characterization gives provenance information as well as conservation and restoration purposes. The prevalence of siliciclastic or carbonate components discriminates between red and yellow bricks, as well as different textures and minerals in the aggregate of the red ones. The mortars are typically pozzolanic, and the aggregate is mostly made up of black and red pozzolanic clasts. In the altar, apse, and aedicule, which constitute the principal place of the Mithraeum, a variety of materials used for the ornamental purpose are represented by pumices, travertine, marble, and limestone. The altar material, catalogued as marble, resulted in being a limestone coated with a white pigment.

**Keywords:** *Mithraeum*; Ostia Antica; archaeological materials; petrography; X-ray diffraction; SEM-EDS

## 1. Introduction

Many ancient buildings characterize Italy. Among them, Roman and religious examples represent a large number. They are commonly hosted on archaeological sites [1,2] that represent open-air museums, buildings directly exposed to the outdoors and a wide variety of environmental stressors. Numerous conservation problems, direct sunlight, rain, area's geology, and adverse weather conditions are just some difficulties that they must face [3]. Focusing on the Roman religious buildings, *Mithraea* are ones that usually are found in Italian archaeological sites [4,5]. The *Mithraeum* term identifies a place dedicated

to the cult of the Persian god Mithra, a sanctuary of this Indo-European god, whose cult expanded rapidly in the 1st-century Roman Empire. They are usually rooms (generally two inter-communicating rooms) obtained from residential complexes or buildings for commercial use. Typically, these places are exposed to the north side [6,7] and are located to the lowest level with the rest of the spaces, to recreate the ritual atmosphere (cold and darkness) simulating the cave of the god [8,9].

Sixteen *Mithraea* (only one of them is a *hypogeum*, so an underground place, the "Terme di Mitra" *Hypogeum*) are found in the archaeological complex of Ostia Antica (Rome) which represents one of the best-known examples of open-air museum present in Italy, together with *Pompeii* and *Herculaneum,* for its entirety. Regarding the state of conservation, very few structures are found in a relatively good state. One of the best examples is the Casa di Diana Mithraeum, a Roman building dated 150 CE [10]. Unfortunately, conservative actions (apart from direct and punctual recovery actions carried out by restores equips) have never been adopted. On the contrary, the state of conservation of this building, such that to develop a strategic conservation plan as result of a multidisciplinary methodology specifically addressed to the wall building materials [11–15]. Recent work has proven how microclimate plays an important role in the conservation state of materials [16]. Here, a full characterization of the other materials is presented to obtain more information on textures and mineralogical/elemental composition. Indeed, what it is also missing is the petrographic/mineralogical characterization of the heterogeneous archaeological materials including both building (e.g., mortar, bricks) and decorative ones (pumice, marble, travertine, ceramic) that are present in the same unsafe microenvironment. In this sense, once investigated all the materials present will be possible to adopt in the future a whole conservation to gain information about the provenance and the social/economic condition (attitude to re-using existing materials or the use of new precious ones).

*Casa di Diana Mithraeum*

The *Casa di Diana* (Figure 1) was built in the central area of Ostia Antica (Region I, Insula III), around 150 CE [10]. It originally had five floors, of which only the ground floor and traces of the continuous balcony of the first floor still survive nowadays. The building is a $40 \times 22$ m rectangular masonry structure with 60 cm wide load-bearing walls and two main corridors.



**Figure 1.** Principal entrance to the "Casa di Diana" *Mithraeum*.

On the northwest side of the ground floor, two-room apartments (*Mithraeum* and *pre-Mithraeum*) of about 50 m$^2$ (27 m$^2$ per each room) are found. The *pre-Mithraeum* served as the proscenium of the Mithraic altar where such a kind of vessel (*dolium*, an earthenware

vase or container used during the sacred rite) at the beginning of the entrance is present. These rooms were constructed with a central aisle flanked on each side by raised seats (podia), located at the height of 50 cm above the floor [17]. They remain as in the past: dark, wet, and cold, i.e., everything to recreate a particular atmosphere for the tauroctony (the killing of the bull). These microclimatic aspects reproduce environmental conditions like "*hypogeum*" [18]. In detail, three areas were distinguished, with different microclimates, within a single *Mithraeum*, and some critical areas (corners and centre of the *Mithraeum* room) where the wall-building materials and the artefacts or decorations are mostly at risk (altar) due to the presence of high relative humidity values together with the non-ventilated area.

In the Mithraeum room, an altar illuminated by a natural spotlight and an aedicule decorated represent the cave of birth of the god Mithra.

The walls are mainly composed of bricks and pozzolanic mortar combined through the opus *caementicium* technique: inner mortar and two outer bricklayers, red/orange and yellow in dispersed order. The latter is a typical Roman construction technique that has revolutionized the history of construction; they consist of full masonry from the intrados to the higher floor, and the *caementa* (the rubble used for the voussoirs, generally pieces of stone the size of a mason's fist) are arranged in strictly horizontal courses [19].

The building is affected by rising damp which causes carbonate and sulphate precipitation, and biological colonization as evidenced by the consumption of mortar and bricks as well as by a typical morphology of degradation by biological growth [12,13,16].

## 2. Materials and Methods

### 2.1. Sample's Collection

Twenty samples, including bricks (6), mortars (4), travertine (1), pumice (3), limestone (2), plasters (2), ceramic (1) and marble (1), are sampled. All these materials come from the *Mithraeum* room except the ceramic sample from the *dolium* collected in the *pre-Mithraeum*. The bricks and mortars constitute the principal wall-building materials, while the other materials come from the different parts of the altar (apse, corbels, aedicule). Table 1 and Figure 2 report the samples' location and the analytical technique applied.

**Table 1.** Typology, sites of sampling and analytical methods carried out. The analytical methodologies are listed with abbreviations. PLM: Polarized Light Microscope; XRD: X-ray Diffraction; SEM: Scanning Electron Microscope.

| Scheme | Material Typology | Sampling Area | Analytical Technique |
|---|---|---|---|
| B1 | Brick | Wall *Mithraeum* at east side | PLM, XRD |
| B2 | Brick | Wall *Mithraeum* at east side | PLM, XRD |
| B3 | Brick | Wall *Mithraeum* at east side | PLM, XRD, SEM |
| B4 | Brick | *Mithraeum* on the north side. Altar (aedicule) | PLM, XRD, SEM |
| B5 | Brick | *Mithraeum* on the north side. Altar (aedicule) | PLM, XRD |
| B6 | Brick | *Mithraeum* on the north side. Altar (corbel) | PLM, XRD |
| M1 | Mortar | Wall *Mithraeum* on the north side | PLM, XRD, SEM |
| M2 | Mortar | *Mithraeum* on the north side. Altar (aedicule) | PLM, XRD, SEM |
| M3 | Mortar | *Mithraeum* on the north side. Altar (aedicule) | PLM, XRD, SEM |
| M4 | Mortar | *Mithraeum* on the north side. Altar (aedicule) | PLM, XRD, SEM |
| P1 | Pumice | *Mithraeum* on the north side. Altar (apse) | PLM, XRD |
| P2 | Pumice | *Mithraeum* on the north side. Altar (apse) | PLM, XRD |
| P3 | Pumice | *Mithraeum* on the north side. Altar (apse) | PLM, XRD |
| T1 | Travertine | *Mithraeum* on the north side. Altar (corbel) | PLM, XRD, ($\delta^{13}$C, $\delta^{18}$O) |
| L1 | Limestone | *Mithraeum* on the north side. Altar (block) | PLM, XRD |
| L2 | Limestone | *Mithraeum* on the north side. Altar (grooved block on the the base of the altar) | PLM, XRD |
| MA1 | Marble | *Mithraeum* on the north side. Altar support (slab resting on top of sample 20) | PLM, XRD |
| C1 | Ceramic | *Dolium. pre- Mithraeum* (right side inside) | PLM, XRD |
| PL1 | Plaster | *Mithraeum* on the north side. Altar (aedicule) | PLM, XRD |
| PL2 | Plaster | *Mithraeum* on the north side. Altar (apse) | PLM, XRD |
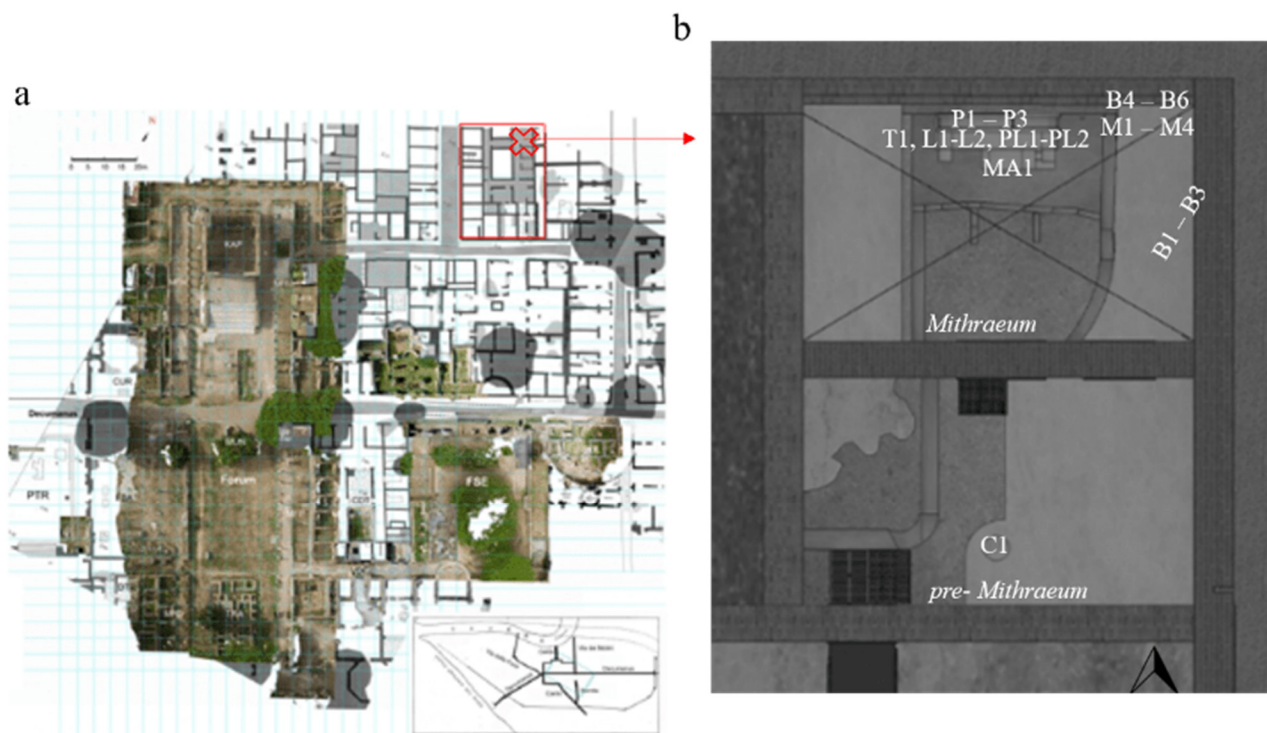
**Figure 2.** Ostia Antica archaeological site. (**a**) Orthophotography [20]. The red box and red cross indicate the "Casa di Diana" with the surrounding area and the *Mithraeum* and *pre-Mithraeum* rooms respectively: (**b**) Plan of the *Mithraeum* and *pre-Mithraeum*. The sample ID are listed in Table 1 (first column).

Bricks of two main colorations are present, a reddish one that is prevalent with respect to a yellowish one. Both the red and yellow bricks are covered by decaying products constituted by gypsum present on the surface of all bricks, and carbonates more abundant in the yellow ones. The masonry surfaces exhibit a whitish patina, exfoliation, cracking, and biological proliferation as an effect of the degradation process.

### 2.2. Instrumentation and Analytical Techniques

Petrographic observations are carried out by Olympus Optical BX60 (Shinjuku, Tokyo, Japan) equipped with a MegaPixel Firewire-Vitana Corporation (PL-A6xx Capture 3.1) camera. Optical microscope observations are performed on thin sections (30 μ thickness). The identification of both predominant and accessory mineral phases [21,22] is carried out by a Siemens D500 X-ray Powder Diffractometer (Munich, Germany) using a monochromatic X-ray beam (Cu–Kα1 X-radiation, 1.54 λ, 40 kV and 20 mA). All the samples are finely grounded and homogenized in an agate mortar and set in a drying cabinet (60 °C) for 24 h.

Scanning electron microscope (SEM) analysis are also performed on the thin section of four mortars and two bricks (representative of the red/orange and yellow typology), coated with a conductive layer (about 200 Å of thickness) of graphite. Back-scattered-electron images (BSE), energy dispersive X-ray (EDS) spectra and X-ray maps are acquired using a FEI-Quanta 400 (SEM–EDAX, Hillsboro, OR, USA), equipped with a 30 kV acceleration voltage Tungsten filament combining high-quality imaging and qualitative elemental analysis.

Finally, for the travertine (T1), isotopic analyses of oxygen and carbon of the $CO_2$ extracted by reaction with 100% $H_3PO_4$ are carried out with a Finnigan Delta Plus mass spectrometer. Isotopic results are expressed in terms of δ‰ and referred to V-PDB standards. The precision of the isotope analyses for the carbonate is ± 0.1 ‰ for both C

and O. The data were normalized to the V-PDP scale using the IAEA standards NBS18 e NBS19 [23].

## 3. Results and Discussion

### 3.1. Bricks

Two main typologies were recognized among the studied bricks, respectively red (B1, B2, B4–B6) and yellow (B3) ones. The red bricks were more compact and better preserved than the yellow brick which displayed a finer, uniform texture and a powdery aspect. Furthermore, the red bricks showed numerous sub-rounded to elongate vesicles (up to 3 mm in diameter) and inclusions of different sizes (up to 4 mm in diameter) and color (brown to black) (Figure 3). The results obtained by petrographic and diffractometric analyses (Figure 4 and Table 2) indicated that samples B1 (Figure 5(a1,2)) and B5 presented a quite fine matrix with a deep brown color and a prevalent siliciclastic aggregate made of quartz and feldspars grains, subordinate opaques, and rare crystals of clinopyroxene and mica. Few black lumps, sometimes including mineral grains likely due to incompletely burned clay portions were also present. Studies refer to the direct effect of temperature (900–1300 °C) and time of burning (2–10 h) of high-calcium limestone samples, as well as the combustion chamber [24,25].
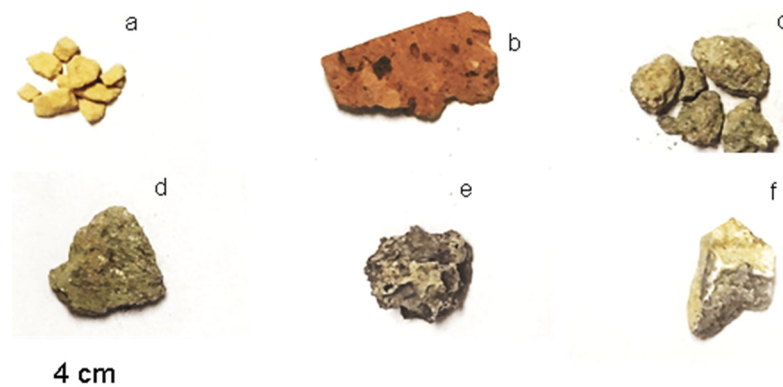


**Figure 3.** Images of macro samples: (**a**) yellow brick, sample B3; (**b**) red brick, sample B4; (**c**,**d**) mortars, samples M1 and M2, respectively; (**e**) pumice, sample P1; (**f**) marble, sample MA1.
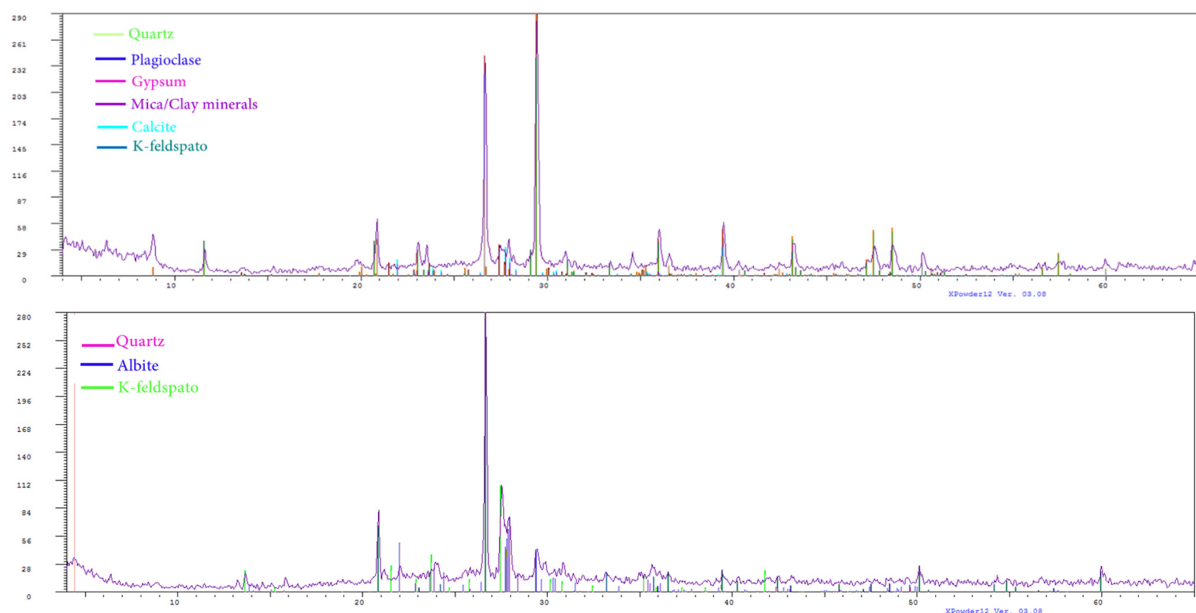


**Figure 4.** Mineralogical composition of representative brick samples for XRD analysis. Upper panel: sample B3 (yellow); below panel: sample B1 (red).

**Table 2.** Mineralogical phases in red and yellow bricks revealed by XRD semi quantitative analyses performed by the XPower12 program. +++ indicated phase abundance in the range 25–20%, ++ 20–15%, + 15–5 %, Tr < 5% and, - undetected. $^{\diamond}$ Indicates the unique yellow brick analyzed.

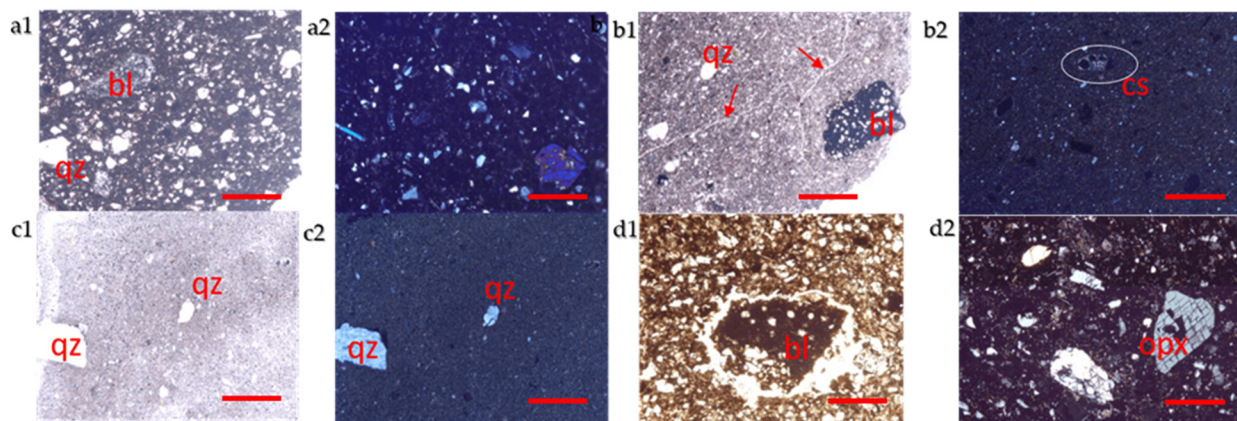| Phases | Sample ID | | | | | |
|---|---|---|---|---|---|---|
| | **B1** | **B2** | **B3** $^{\diamond}$ | **B4** | **B5** | **B6** |
| Amorphous phases | + | ++ | +++ | +++ | + | + |
| Quartz | +++ | ++ | ++ | ++ | +++ | + |
| Calcite | + | ++ | +++ | + | + | - |
| Dolomite | - | - | - | - | - | + |
| Plagioclase feldspar | ++ | + | + | + | ++ | ++ |
| Pyroxene | + | Tr | - | + | - | Tr |
| Mica | - | + | + | + | Tr | + |
| Analcime | - | Tr | - | - | - | - |
| Alkaline feldspar | +++ | + | + | ++ | +++ | ++ |
| Hematite | Tr | + | - | Tr | Tr | - |
| Gypsum | - | ++ | + | - | - | - |
| Clay minerals | | + | | + | | |



**Figure 5.** Microphotographs of brick samples. (**a**) sample B1; (**b**) sample B2; (**c**) sample B3 (yellow); (**d**) sample B4; a1, b1 c1 and d1 plane polarized light; a2, b2, d2, c2 crossed polarized light. All microphotographs are at 4× magnifications. bl = black lump; cs = carbonate shell; opx = orthopyroxene; qz = quartz; red arrows indicate firing stress lines. Line red bar = 1 mm.

The sample B2 (Figure 5(b1,2)) presented a finer and more homogenous matrix than the previous ones, with a pale brown color. Moreover, the matrix seemed to have suffered evident firing stress (Figure 5(b1)). The aggregate was very scarce and composed primarily by crystals of quartz and occasional black lumps, which include several grains of quartz and alkaline feldspar (Figure 5(b1)) and isolated carbonate shells (Figure 5(b2)).

Among the red bricks sample, B2 contains gypsum, abundant calcite, and clay minerals (Table 2). Samples B4 and B6 presented a medium-grained matrix with a pale brown-reddish color, constituted prevalently by siliciclastic minerals, i.e., numerous quartz and feldspars crystals. Some prismatic white crystal of orthopyroxene with orthogonal cleavage, as well as black lumps, were also present (Figure 5(d2)) as the coarser aggregate fraction, together with laths of phyllosilicates (mica) and clay minerals (Figure 6, Table 2). XRD (Table 2) and SEM analyses also revealed the presence of a small amount of calcite in sample B4, and dolomite in sample B6 (Table 2).
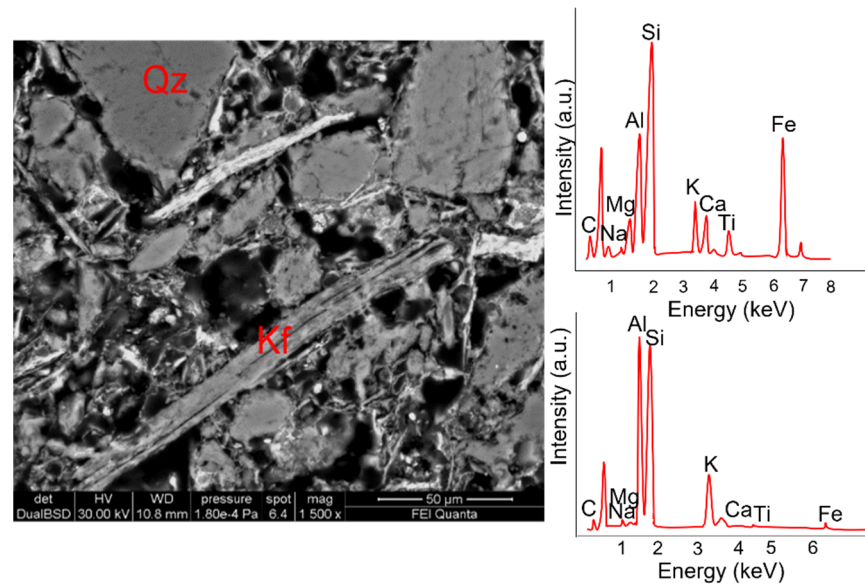
**Figure 6.** SEM image and EDS spectra of amphibole (upper spectrum on the right) and clay mineral (lower spectrum on the right) referred to sample B4 (red brick).

Sample B3, the only yellow brick collected, displayed a microstructure with a very scarce aggregate fraction and a very fine matrix (Figure 5(c1,2)). The pale ochre color of the matrix was likely due to the abundant calcite fraction, as revealed by XRD analyses (Table 2) and by SEM analysis (Figure 6). However, BSE image and X-ray maps evidenced a certain heterogeneity in the carbonate content of the matrix. A small amount of gypsum was recognized also in this sample. Crystals of quartz are present in the scarce aggregate fraction, and X-ray maps (Figure 7) revealed the presence of minute grains of Fe oxides.
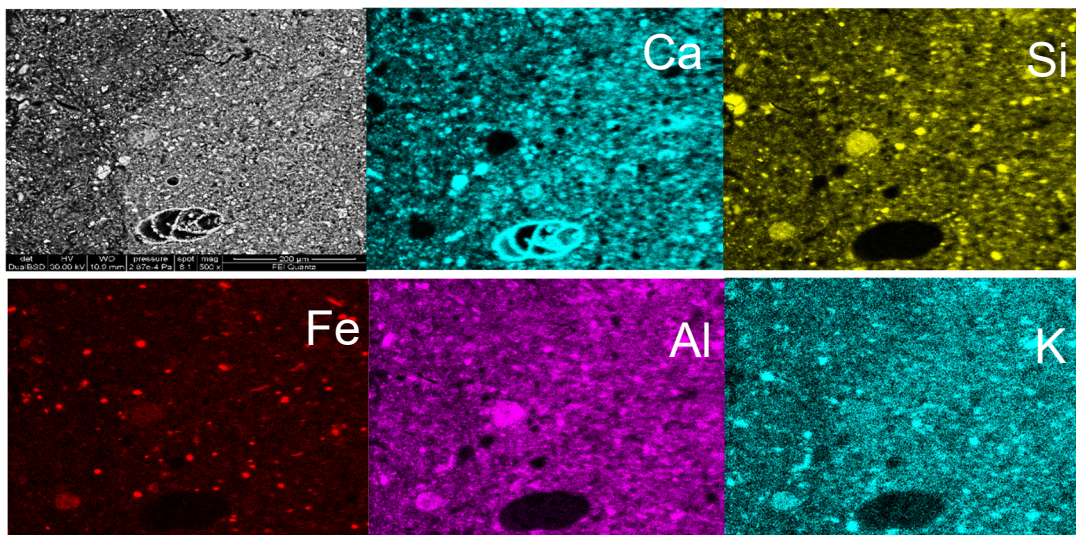


**Figure 7.** X-ray elemental maps of sample B3, yellow brick (Ca, Si, Fe, Al and K respectively).

In summary, the matrix color goes from deep brown to brown reddish. Red bricks display a significant variability in texture, color, and relative abundance of a siliciclastic component. Samples B1 and B5 are similar and characterized by the higher abundance of quartz and feldspars, whereas sample B4 is characterized by a higher amount of phyllosilicates. Sample B6 has a different texture with a minor, but coarser-grained aggregate fraction and dolomite as carbonate phase. Sample B2 is described by the fewer abundance of silicates phases and by the more abundant carbonate fraction. For this last aspect, it is

like sample B3 which displays a pale ochre color, a homogeneous, mostly carbonate matrix with fewer and smaller siliciclastic minerals.

### 3.2. Mortars

The petrographic results obtained by PLM analyses suggest that the mortars are typical of the pozzolanic nature [26], being the pozzolanic clasts and their mineral phases. As for analcime and clinopyroxene, the principal constituents of the aggregate fraction can be seen in Figure 8.
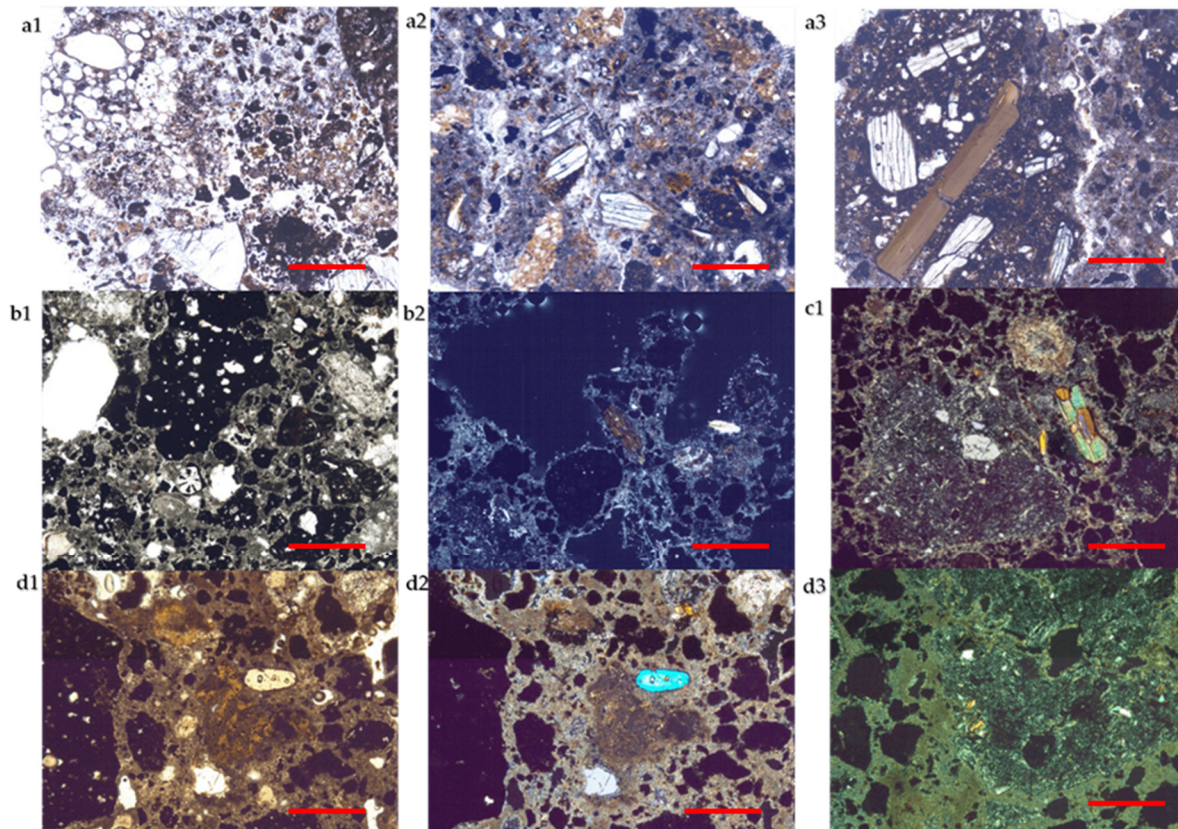


**Figure 8.** Microphotographs of mortar samples. (**a**) Sample M1 (a1: plane polarized light, a2, a3 crossed polarized light): fragments of pumice and black/red pozzolan are shown; (**b**) sample M2 (b1: plane polarized light, b2: crossed polarized light); (**c**) sample M3 (c1: crossed polarized light); (**d**) sample M4 (d1: plane polarized light, d2–d3: crossed polarized light). All microphotographs are at 4× magnifications. Line red bar = 1 mm.

Specifically, sample M1 has an aggregate displaying heterogeneous size and shape of fragments; the larger clasts are formed mainly by both red and black pozzolan, characterized, respectively, by low and high porphiricity index [27], and subordinately by pumice. Smaller fragments are represented by pozzolan clasts and single crystals (mainly pyroxene) and rare (analcimized) leucite derived from the crush of pozzolan. Leucite (analcimized) is also present as microcrystals as testified by XRD results (Table 3). Mica and occasional quartz are present. Some silicate lumps, described below, are also recognized in this mortar (Figure 5(a1)) as well as in samples M3 and M4. The binder-aggregate ratio is approximately 1:3 (Figure 9). Binder is of a carbonate nature, as testified by XRD data and X-ray maps; it includes lime lumps, not blended in the mixture, due to the defect of carbonation or heterogeneity of the lime itself (Figure 9. The binder/pozzolan fragments interface is characterized by reaction phenomena (Figure 8(a3)).

**Table 3.** Main mineralogical phases in the mortars revealed XRD semi quantitative analyses performed by the XPower12 program. +++ indicated phases abundance in the range 25–20%, ++ 20–15%, + 15–5 %, Tr < 5% and, - undetected.

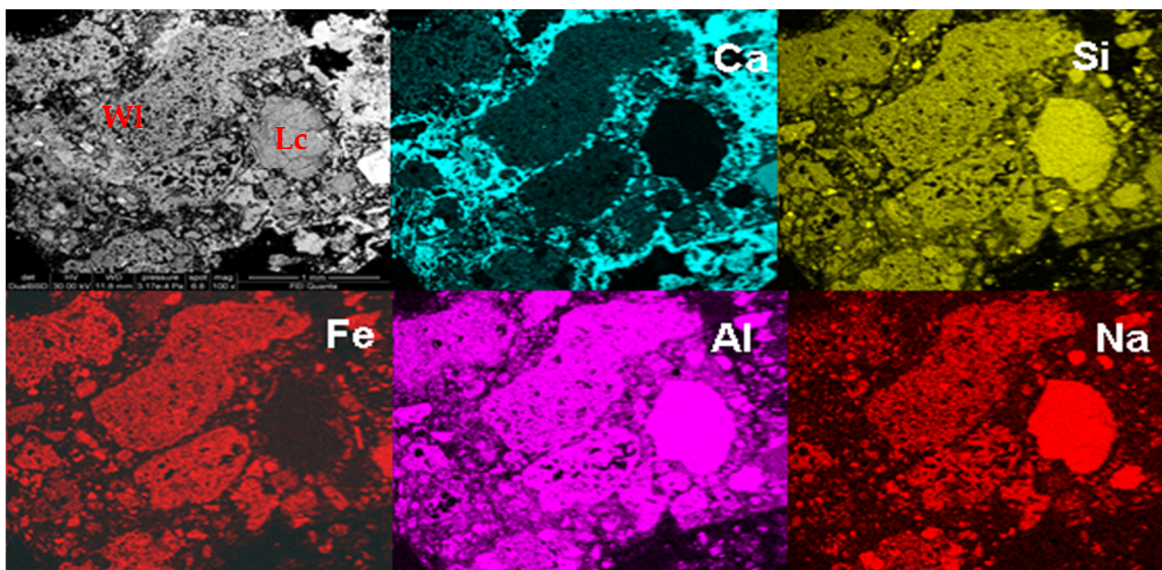| Phases | Sample ID | | | |
|---|---|---|---|---|
| | M1 | M2 | M3 | M4 |
| Amorphous phases | +++ | ++ | ++ | +++ |
| Quartz | Tr | Tr | - | - |
| Calcite | +++ | ++ | +++ | ++/+++ |
| Clinopyroxene | ++ | ++ | +/++ | +/++ |
| Mica | ++ | - | + | - |
| Analcime | +++ | +++ | ++ | +++ |
| Chlorite | Tr | - | - | - |
| Hematite | - | Tr | - | - |



**Figure 9.** BSE image and X-ray maps of sample M1. Fragments of red pozzolan, a crystal of analcimized leucite (Lc) and lime lump (Wl) are indicated.

Sample M2 presented an aggregate with a very heterogeneous particle size, in which fragments of red pozzolan with small cartwheel leucite crystals in the groundmass prevail (Figure 9). Isolated crystals of clinopyroxene and leucite, lava fragments, and occasional quartz crystals were also present.

Numerous, coarse silicate lumps were found, having a soil-like aspect such as that shown in Figures 9 and 10. Similar silicate lumps have been recognized in 'non-pozzolanic' mortars in Southern Italy [28] and have been interpreted as incomplete mixtures of carbonate and silicate binder materials. In this work, they could represent alteration products of the volcanics of the roman area (scoria, pumice, tuff). Indeed, the EDS spectra of these lumps are like those of the scoria and pumice matrix recognized in the study of mortars (Figure 11).
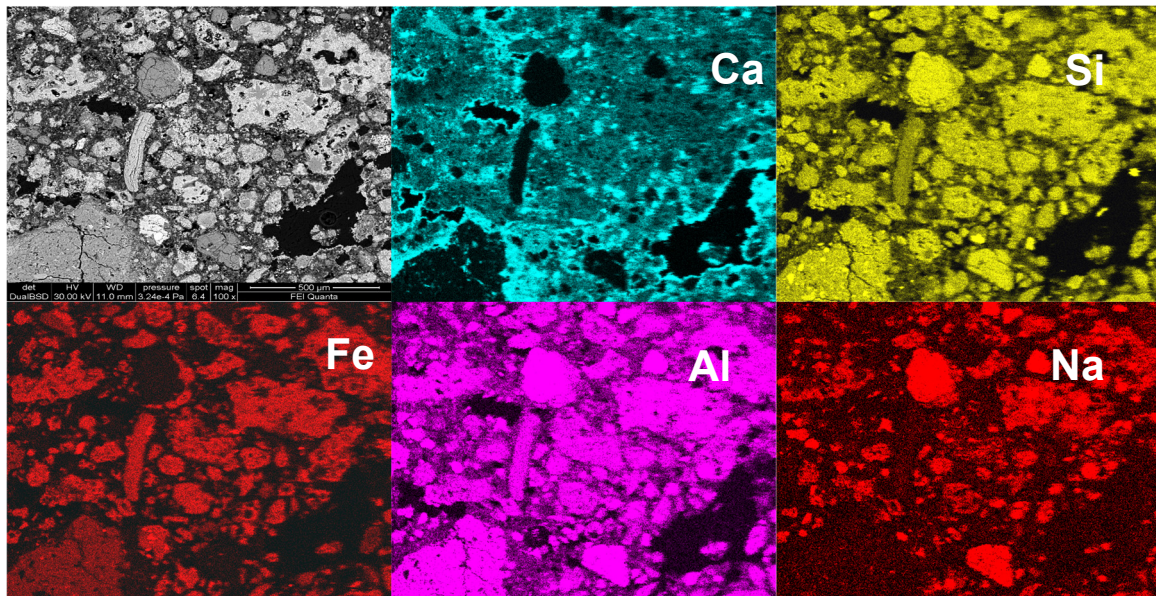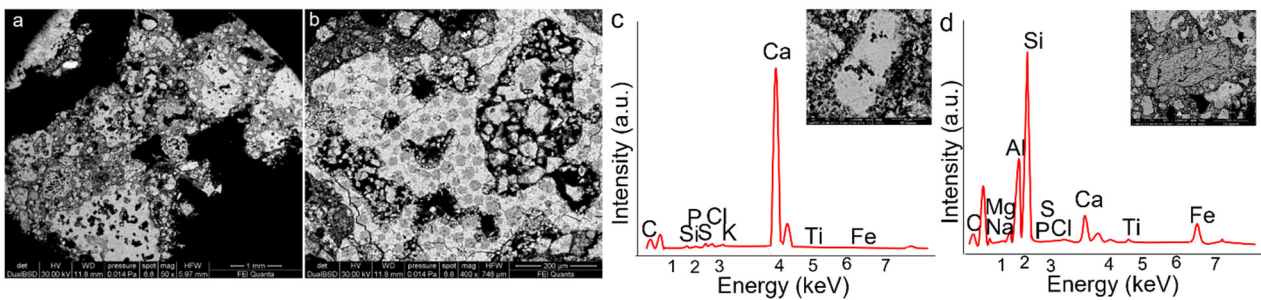
**Figure 10.** BSE image and X-ray maps of the sample M2.



**Figure 11.** SEM images (**a**–**d**) of the sample M3 showing fragments of red pozzolan rich in analicimized leucite (**b**). In (**c**,**d**) details of the carbonate and clay minerals lumps are reported EDS with the respective EDS spectra.

The binder-aggregate ratio was higher than in sample M1, and the carbonate matrix presented a heterogeneous color (Figure 8(b1,b2)) and cooking residues consisting of lime lumps (Figure 9).

Sample M3 presented an aggregate with variously sized pozzolanic fragments, rarer silicate lumps, few large crystals of mica, analcime and occasional quartz (Figure 8(c1); Figure 11). The binder had a carbonate-aluminosilicate composition (Figure 11d), and its ratio with respect to the aggregate was about 1:3.

Finally, sample M4 presented an aggregate with a bimodal distribution of the grain size; the larger fragments were formed principally of pozzolanic clasts, rare fragments of lava and silicate lumps (Figure 8(d1–d3)). The finer fraction was constituted by rare minerals resulting from crushed pozzolanic materials (essentially pyroxene and analcime), smaller lava fragments (<400 mμ) and occasional crystals of quartz (Figures 12 and 13, Table 3). The binder consisted of a mixing of carbonate-aluminosilicate components, representing the marl fraction of the carbonate used to make lime (Figure 12). A reaction layer linked to hydraulic reactivity [29] was identified between quartz grain and both carbonate and clay fractions of the binder, which produced calcium silico-aluminate phases with high silica and low calcium content (Figure 12). A binder-aggregate ratio more elevated than in the other samples and close to 1:2 was found.
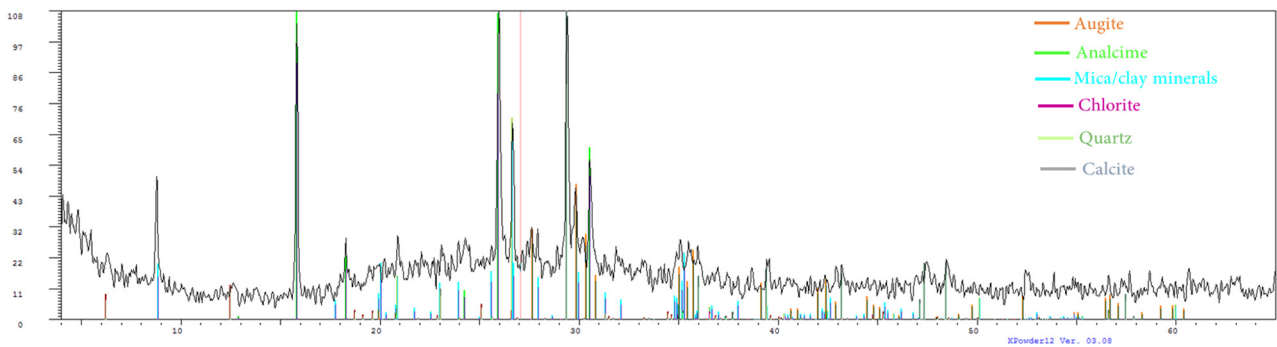
**Figure 12.** Mineralogical composition of M4 sample representative pozzolanic mortars.
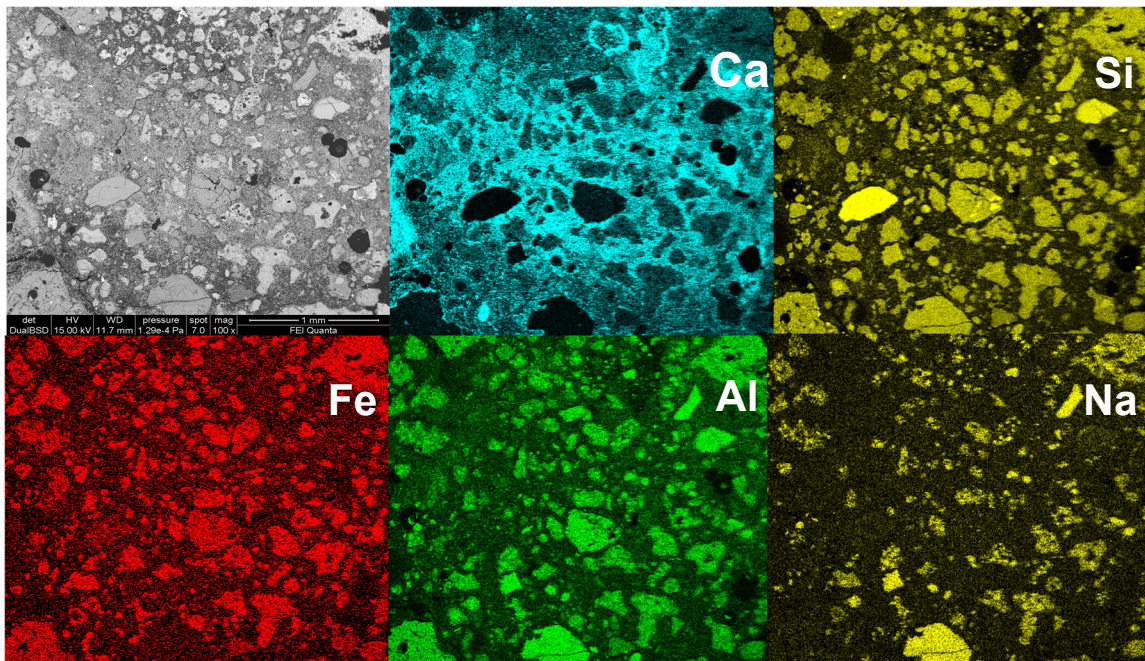


**Figure 13.** BSE image and X-ray maps of sample M4.

The XRD results (Table 3) detail what followed the optical microscope observations. Indeed, the mineral phases that dominated were analcime and clinopyroxene, which were typical of pozzolans. The amorphous material, mostly referable to the glass fraction in the pozzolanic fragments, was more abundant in sample M4, whereas fragments of red pozzolans were more abundant in the glass.

*3.3. Other Materials*

Regarding the other sampled materials (pumice, travertine, limestone, marble, ceramic and plasters), petrographic observation and XRD analysis are reported in Figure 14 and Table 4, respectively.
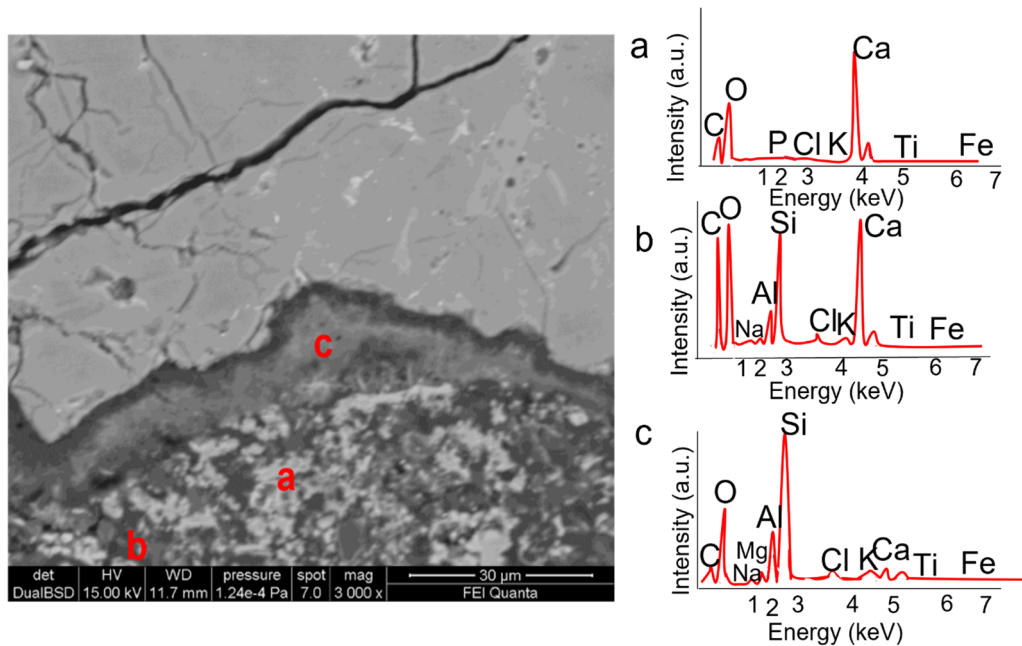
**Figure 14.** BSE image and EDS spectra of binder components (**a**,**b**) and reaction edge between quartz crystal and binder (**c**).

**Table 4.** Main mineralogical phases in the pumices (P1, P2, P3), travertine (T1), limestone (L1, L2), marble (MA1), ceramic (C1) and plaster (PL1, PL2) revealed by XRD analysis. +++ Abundant, ++ Present, + Small amount, Tr. Traces, - Undetected. * Gypsum.

| Phase | Sample ID | | | | | | | | | |
|---|---|---|---|---|---|---|---|---|---|---|
| | **P1** | **P2** | **P3** | **T1** | **L1** | **L2** | **MA1** | **C1** | **PL1** | **PL2** |
| Amorphous phases | ++ | ++ | +++ | - | - | - | - | - | - | - |
| Calcite | - | Tr | + | +++ | +++ | +++ | +++ | + | +++ | +++ |
| Quartz | - | - | - | - | - | - | - | + | - | - |
| Dolomite | - | - | - | - | - | - | Tr | - | - | - |
| Plagioclase feldspar | +++ | ++ | + | - | - | - | - | ++ | - | - |
| Augite | +++ | ++ | ++ | - | - | - | - | + | - | - |
| Mica | + | + | Tr | - | - | - | - | + | - | - |
| Analcime | Tr | - | - | - | - | - | - | - | - | - |
| Hematite | + | Tr | Tr | - | - | - | - | - | - | - |
| Alkali feldspar | - | ++ | ++ | - | - | - | - | ++ | - | - |
| Putonarite | - | - | - | - | Tr | - | - | - | - | - |
| Lanarkite | - | - | - | - | Tr | - | - | - | - | - |
| Gypsum | Tr * | Tr * | Tr * | - | - | - | - | Tr | - | - |

The highly vesiculated pumices samples (Figure 15a–c) were characterized by the presence of pyroxene and feldspars as main phenocryst phases and abundant glassy groundmass. To better imitate the cave where the Mithra was born, the pumice (applied on a layer of gypsum—as was found by XRD analysis—Table 4) was also painted with a blue pigment (as can be observed on a pumice piece—Figure 13). Indeed, it is well-known that the god Mithra is linked to the sky and astronomy.
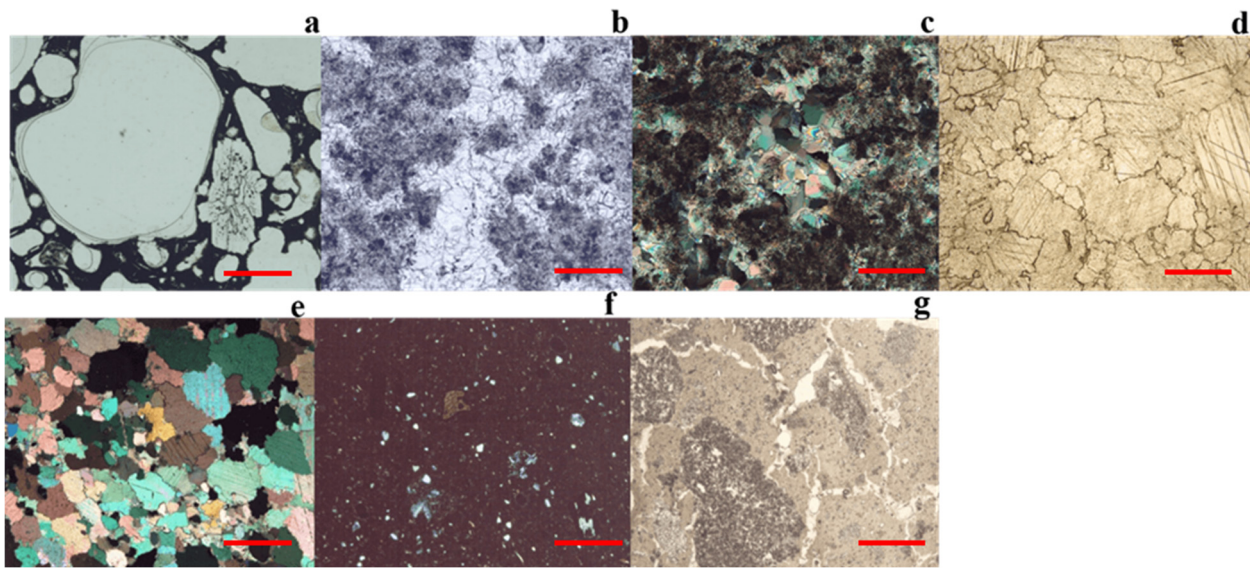
**Figure 15.** Microphotographs of: (**a**) sample P1, pumice; (**b**) sample T1, travertine; (**c**) sample L2, limestone; (**d**) sample MA1, marble; (**e**) sample C1, ceramic; (**f**) sample PL1, plaster; (**g**) Micas represented accessory minerals. All the microphotographs are at plane polarized light, except than c and d2 that are at crossed polarized light. All the samples are investigated at 4× magnifications. Line red bars = 1 mm.

Sample T1 was identified as travertine based on petrographic observation and XRD analysis (calcite) (Figure 15d; Table 4). Isotopic results (expressed in terms of δ‰ and referred to PDB standard) were $\delta\ ^{13}C_{PDB} = 10.08$‰ and $\delta\ ^{18}O_{PDB} = -6.34$‰, These values are typical values for the travertine of Tivoli [30,31]. Therefore, although other origins cannot be completely excluded, they are presumably less likely, and we can realistically consider that the T1 travertine comes from the large travertine quarries of Tivoli that are very close to Ostia.

Sample L1 had an inventory number corresponding to "marble altar". Petrographic analysis of its thin section showed a fine heterogeneous matrix with scattered crystals of calcite and other minerals (Figure 15e). XRD analysis revealed the presence of lanarkite $(Pb_2(SO_4)\ O)$ and putoranite, $(Cu\ (Fe,\ Ni)_2S_2)$. These observations suggested that the material is not a marble, but probably a limestone coated with a white pigment.

Regarding sample L2, microscopic observation revealed a microcrystalline structure, presenting vugs surrounded by larger crystals aggregates consisting of recrystallized calcite. The presence of widespread graphite pointed toward the identification of the sample as a carbonaceous limestone (Figure 15f). The presence of calcite confirms this as the only mineral phase revealed by XRD.

Sample MA1 was a medium-grained marble that exhibited a typical grey color banding and emitted a distinct sulphur odor when scraped or grinded. Observations at PLM revealed a granoblastic texture with the typical rhombohedral cleavage of calcite crystals, which did not show any preferred orientation. Grain size varied from medium to fine (0.1–5 mm), and contacts between grains formed 120° triple junctions. Micas represented accessory minerals (Figure 15g). The combination of these features is strongly indicative of a Proconnesian provenance [32].

Sample C1 was a ceramic characterized by a compact microstructure with low aggregate/binder ratio. The aggregate was made by siliciclastic minerals consisting of plagioclase and alkali feldspar with subordinate pyroxene, mica and quartz (Figure 13, Table 3).

For the last samples, PL1 and PL2, XRD revealed the presence of calcite as the only crystalline phase. They represent plasters, which microscopic observation on thin-sections display some differences in the structure and texture (Figure 13).

## 4. Conclusions

The combined use of PLM, XRD and SEM-EDS techniques, represent a powerful approach in the materials' characterization in that it highlighted some interesting issues.

Two main colorations of bricks are present, a reddish one that is prevalent with respect to a yellowish one. Both the red and yellow bricks were covered by decaying products like gypsum present on the surface; carbonates were more abundant in the yellow ones. The wall building materials surface exhibited a whitish patina, exfoliation, cracking, and biological proliferation effects of the accelerated degradation process.

Differences in the microstructure and aggregate type, between the red/orange and yellow bricks investigated, as well as among the same red/orange bricks, were found. The difference between the red/orange and the yellow bricks was also macroscopically observed at first sight on feature walls where the red/orange bricks, predominant on the yellow ones, appeared to be more compact and in a better state of conservation. Indeed, amounts of gypsum and calcite were recognized mostly in the yellow bricks, pointing out the action of damping water in the origin of these secondary minerals.

Regarding the differences found among the red/orange bricks, PLM and XRD results pointed out that they consist in the matrix color (from deep brown to brown reddish), in their textures (characterized by different matrix/temper ratio and quartz/feldspar ratio into the siliciclastic aggregate), and in variable amount of black lumps. Moreover, some red/orange bricks were characterized by the less abundance of silicates phases and by the more abundant carbonate fraction, which made them more like the yellow brick. These aspects represent an interesting clue, perhaps related to the nature of the clay and temper, kiln environment, and the temperature of the firing process. These results, together with the use of the *opus caementicium* technique, provoke a lot of thinking about the hypothesis of the different historic periods of the bricks, the Byzantine for the yellow bricks.

Second, PLM, SEM-EDS and X-ray maps allowed us to establish the nature of mortars. That is a pozzolanic mortar characterized by pozzolanic fragments and mineral phases as analcime and clinopyroxene, which resulted from crushed pozzolan. The binder-aggregate ratio was low (approximately 1:3); the binder results in mixing between aluminosilicate and carbonate components. Cooking residues consisting of lime lumps were also found. Moreover, reaction phenomena were observed in silicate minerals (analcime and quartz), underlying the well-known hydraulic property of this kind of materials.

Among the decorative materials considered, we found that the Mithraic altar, previously recorded as marble, resulted in being made by a carbonaceous limestone coated with a white pigment. Moreover, stable isotopes results led to assume that the travertine constituting the corbel came from nearby Tivoli deposits. Finally, the block at the base of the altar resulted in being made by a Proconnesian marble. These results suggest that in agreement with that observed in other *Mithraea* present in Ostia Antica as well as in the "Casa di Diana" *Mithraeum* only poor materials were employed for decorative purposes. Indeed, the only marble present in the Diana *Mithraeum* supported of the altar and was clearly a piece reused. This agrees with knowledge about Mithraism as a religion predicated also among the poor social classes [33].

The results show how, despite its apparent "integrity", the building needs a rescue intervention. Phenomena like recrystallized calcite, incomplete mixture of carbonate (reaction layer linked to hydraulic reactivity) and incompletely burned clay portions found are associated with both poor materials used (wall-building materials) or reuse materials, typical of the *opus caementicium* technique, and accelerate carbonation phenomena (of secondary formation) due to the microenvironmental condition and biological proliferation. The latter can be easily solved with the removal of the biological apparatus as a temporary remedy to then make actions such as the installation of filters on the window and a turnout control.

Regarding the restoration actions, by knowing how the raw materials are made, it is possible to fill the gaps and the fracture with appropriate materials with the same composition.

## References

1. Laurenti, M.C. *Le Coperture Delle Aree Archeologiche: Museo Aperto*; Gangemi Editore SpA: Rome, Italy, 2006.
2. Dey, T.; Carter, J.C.; Swift, K. SEM-EDX and FTIR analysis of archaeological ceramic potteries from southern Italy. *Microscopy* **2020**, *69*, 371–380. [CrossRef]
3. Lucchi, E. Multidisciplinary risk-based analysis for supporting the decision making process on conservation, energy efficiency, and human comfort in museum buildings. *J. Cult. Herit.* **2016**, *22*, 1079–1089. [CrossRef]
4. Canciani, V. Revising an archaeological context through archival excavation: The Duino Mithraeum as a case study. In Proceedings of the Humanities in the Third Millennium: Approaches, Contamination and Perspectives, Verona, Italy, 17 October 2019; Cierre Edizioni: Pescia, Italy, 2020; pp. 15–26.
5. Frasca, F.; Verticchio, E.; Caratelli, A.; Bertolin, C.; Camuffo, D.; Siani, A.M. A Comprehensive Study of the Microclimate-Induced Conservation Risks in Hypogeal Sites: The Mithraeum of the Baths of Caracalla (Rome). *Sensors* **2020**, *20*, 3310. [CrossRef] [PubMed]
6. Sclavi, S.; Monaco, M.; Carnevale, F.; Ranieri, M.; Gaudenzi, S.; Polcaro, F.V.; Scatigno, C. The orientation of the Mithraea in Ostia Antica. *Mediterr. Archaeol. Archaeom.* **2016**, *16*, 4.
7. Sparavigna, A.C. *On the Astronomical Orientation of Mithraea*; Department of Applied Science and Technology, Politecnico di Torino: Turin, Italy, 2017.
8. Martin, L.H. Seeing the Mithraic taurocytony. *Numen* **2021**, *68*, 357–381. [CrossRef]
9. Rubio, R. Multisensory Experiences in Mithraic Initiation. In *SENSORIVM: The Senses in Roman Polytheism*; Brill: Leiden, The Netherlands, 2021; pp. 177–191. [CrossRef]
10. Available online: https://www.ia-ostiaantica.org/news/il-caseggiato-di-diana/ (accessed on 19 July 2021).
11. Scatigno, C. An Innovative Multidisciplinary Methodology to Evaluate the Conservation State of Cultural Sites as a Whole: Casa di Diana (Ostia Antica, Italy). 2017. Available online: https://addi.ehu.es/handle/10810/21565 (accessed on 19 July 2021).
12. Cardarelli, E.; De Donno, G.; Oliveti, I.; Scatigno, C. Three-dimensional reconstruction of a masonry building through electrical and seismic tomography validated by biological analyses. *Near Surf. Geophys.* **2018**, *16*, 1–13. [CrossRef]
13. Scatigno, C.; Moricca, C.; Tortolini, C.; Favero, G. The influence of environmental parameters in the biocolonization of the Mithraeum in the roman masonry of casa di Diana (Ostia Antica, Italy). *Environ. Sci. Pollut. Res.* **2016**, *23*, 13403–13412. [CrossRef]
14. Scatigno, C.; Prieto-Taboada, N.; Martinez, M.P.; Conte, A.M.; Madariaga, J.M. A non-invasive spectroscopic study to evaluate both technological features and conservation state of two types of ancient Roman coloured bricks. *Spectrochim. Acta Part A Mol. Biomol. Spectrosc.* **2018**, *204*, 55–63. [CrossRef]
15. Scatigno, C.; Prieto-Taboada, N.; García-Florentino, C.; de Vallejuelo, S.F.O.; Maguregui, M.; Madariaga, J.M. Combination of in situ spectroscopy and chemometric techniques to discriminate different types of Roman bricks and the influence of microclimate environment. *Environ. Sci. Pollut. Res.* **2018**, *25*, 6285–6299. [CrossRef]
16. Scatigno, C.; Prieto-Taboada, N.; Festa, G.; Madariaga, J.M. Soluble Salts Quantitative Characterization and Thermodynamic Modeling on Roman Bricks to Assess the Origin of Their Formation. *Molecules* **2021**, *26*, 2866. [CrossRef] [PubMed]
17. Clauss, M. *The Roman Cult of Mithras: The God and His Mysteries*; Routledge: London, UK, 2017.

18.  Scatigno, C.; Gaudenzi, S.; Sammartino, M.P.; Visco, G. A microclimate study on hypogea environments of ancient roman building. *Sci. Total Environ.* **2016**, *566*, 298–305. [CrossRef]
19.  Sinopoli, A.; Danila, A. The Dome of the Temple of Diana in Baiae: Opus Caementicium, Geometry and Mechanics. *Int. J. Archit. Herit.* **2021**, 1–32. [CrossRef]
20.  Gering, A. Le ultime fasi della monumentalizzazione del centro di Ostia tardoantica. Attività della missione della Humboldt-Universität di Berlino tra il 2009 e il 2013. *Mélanges l'École Française Rome-Antiq.* **2014**, *126-1*. [CrossRef]
21.  Yaseen, I.A.B.; Al-Amoush, H.; Al-Farajat, M.; Mayyas, A. Petrography and mineralogy of Roman mortars from buildings of the ancient city of Jerash, Jordan. *Constr. Build. Mater.* **2013**, *38*, 465–471. [CrossRef]
22.  Aloise, P.; Ricca, M.; La Russa, M.F.; Ruffolo, S.A.; Belfiore, C.M.; Padeletti, G.; Crisci, G.M. Diagnostic analysis of stone materials from underwater excavations: The case study of the Roman archaeological site of Baia (Naples, Italy). *Appl. Phys. A* **2014**, *114*, 655–662. [CrossRef]
23.  Coplen, T.B. New guidelines for reporting stable hydrogen, carbon, and oxygen isotope-ratio data. *Geochim. Cosmochim. Acta* **1996**, *60*, 3359–3360. [CrossRef]
24.  Ray, K.W.; Mathers, F.C. Effect of Temperature and Time of Burning upon the Properties of High–Calcuim Lime1. *Ind. Eng. Chem.* **1928**, *20*, 415–419. [CrossRef]
25.  Robinson, H.O.; Christopher, S. Apparatus and Method for Brick-Burning. U.S. Patent No. 1,367,756, 8 February 1921.
26.  Pecchioni, E.; Fratini, F.; Cantisani, E. *Atlas of the Ancient Mortars in Thin Section under Optical Microscope*; Nardini Editore: Florence, Italy, 2014; Volume 78.
27.  Marra, F.; Danti, A.; Gaeta, M. The volcanic aggregate of ancient Roman mortars from the Capitoline Hill: Petrographic criteria for identification of Rome's "pozzolans" and historical implications. *J. Volcanol. Geotherm. Res.* **2015**, *308*, 113–126. [CrossRef]
28.  Conte, A.M.; Corda, L.; Esposito, D.; Giorgi, E. Characterization of mortars from the medieval Abbey of Cerrate (southern Italy). *J. Archaeol. Sci. Rep.* **2017**, *12*, 463–479. [CrossRef]
29.  Moropoulou, A.; Bakolas, A.; Anagnostopoulou, S. Composite materials in ancient structures. *Cem. Concr. Compos.* **2005**, *27*, 295–300. [CrossRef]
30.  Manfra, L.; Masi, U.; Turi, B. La composizione isotopica dei travertini del Lazio. *Geol. Rom.* **1976**, *15*, 127–174.
31.  Minissale, A.; Kerrick, D.M.; Magro, G.; Murrell, M.T.; Paladini, M.; Rihs, S.; Vaselli, O. Geochemistry of Quaternary travertines in the region north of Rome (Italy): Structural, hydrologic and paleoclimatic implications. *Earth Planet. Sci. Lett.* **2002**, *203*, 709–728. [CrossRef]
32.  Attanasio, D.; Brilli, M.; Bruno, M. The properties and identification of marble from Proconnesos (Marmara Island, Turkey): A new database including isotopic, EPR and petrographic data. *Archaeometry* **2008**, *50*, 747–774. [CrossRef]
33.  Pavia, C. *Roma Mitraica*; C. Lorenzini: Pescia, Italy, 1986.